# Registration-based lung tissue mechanics assessment during tidal breathing

Kai Ding[1], Kunlin Cao[2], Shalmali V. Bodas[1], Gary E. Christensen[2]
Eric A. Hoffman[3,1], and Joseph M. Reinhardt[1]

[1] Department of Biomedical Engineering
[2] Department of Electrical and Computer Engineering
[3] Department of Radiology
The University of Iowa, Iowa City, IA 52242

{kai-ding, kunlin-cao, shalmalividyadhar-bodas, gary-christensen,
eric-hoffman,joe-reinhardt}@uiowa.edu

**Abstract.** Lung tissue expansion and contraction can be assessed by acquiring multiple 3D CT images at different lung volumes. Static "breath-hold" imaging has been shown to produce tissue deformation estimates that match well with other measures of lung function. However, dynamic imaging protocols that image the breathing lung may produce more physiologically meaningful estimates of lung function. We use non-linear image registration to match retrospectively reconstructed respiratory-gated lung "dynamic" CT volumes acquired during tidal breathing. We compare the lung expansion and contraction estimates from the dynamic acquisitions to regional ventilation assessed by xenon-enhanced CT. The Jacobian-based lung volume change estimate shows a good agreement with the xenon-CT (average $r^2 = 0.85$) at image pair acquired at 50% and 75% of the inspiration duration.

## 1 Introduction

The lungs expand and contract during the respiratory cycle. Lung tissue mechanics depends on the material properties of the lung parenchyma and the mechanical inter-relationships between the lungs, diaphragm, and other parts of the respiratory system. Pulmonary diseases, such as fibrosis and emphysema, can change the tissue material properties of lung parenchyma and the associated lung function.

Lung tissue expansion and contraction can be assessed by acquiring multiple 3D CT images at different lung volumes. Static "breath-hold" imaging has been shown to produce tissue expansion estimates that match well with other measures of lung expansion [1]. However, static imaging is not able to observe kinematic effects, and dynamic imaging protocols that image the breathing lung may produce more physiologically meaningful estimates of lung function.

Various efforts have been made to non-invasively assess lung function. Guerrero et al. have used optical-flow registration to compute lung ventilation from 4D CT [2, 3]. Gee et al. have used non-rigid registration to study pulmonary

kinematics [4] using magnetic resonance (MR) imaging. Christensen et al. have used image registration to match images across cine-CT sequences and estimate rates of local tissue expansion and contraction [5]. While they were able to show that their accumulated measurement matched well with the global measurement, they were not able to compare the registration-based measurements to local measures of regional tissue ventilation. Others have used hyperpolarized gas MR imaging of the lung to assess lung function and to demonstrate pathophysiological changes [6]. Xenon-enhanced CT (Xe-CT) has been used to measure regional ventilation by observing the gas wash-in and wash-out rate on serial CT images [7–9]. All of these approaches have some disadvantages, including limited spatial coverage, limited spatial resolution, high cost, or the need for special equipment or personnel.

We have previously shown a good correlation (linear regression, average $r^2 = 0.73$) between specific ventilation measured from Xe-CT and specific volume change assessed by image registration [1]. By applying 3D registration to CT images of the lung acquired at different levels of inflation (static breath-hold imaging), we estimate the regional lung expansion from the displacement field calculated from the image registration. We compared these lung expansion estimates to Xe-CT derived measures of regional ventilation to validate our measurements and to establish their physiological significance.

However, it is reasonable to think that the static breath-hold scenario does not fully depict the behavior and function of the moving, breathing lung. Dynamic imaging, where images are acquired across the respiratory cycle, may provide better estimates of lung mechanics, and may more accurately reflect the behavior of the breathing lung. In this paper we compare registration-based estimates of lung mechanics derived from dynamic imaging protocols to Xe-CT estimates of lung ventilation and evaluate the accuracy of the registration applied in this study.

## 2 Materials and Methods

### 2.1 Data Acquisition

Appropriate animal ethics approval was obtained for these protocols from the University of Iowa Animal Care and Use Committee and the study adhered to NIH guidelines for animal experimentation. Four adult sheep were used for experiments. The sheep were anesthetized using intravenous pentobarbital and mechanically ventilated during experiments. The dynamic respiratory-gated CT images are acquired with the animals in the supine position using the dynamic imaging protocol with a pitch of 0.1, slice collimation of 0.6 mm, rotation time of 0.5 sec, slice thickness of 0.75 mm, slice increment of 0.5 mm, 120 kV, 400 mAs, and kernel B30f. Images are reconstructed retrospectively at 0, 25, 50, 75, and 100% of the inspiration duration and 75, 50 and 25% of the expiration duration (herein denoted as the $T0$, $T1$, $T2$, $T3$, $T4$, $T5$, $T6$, and $T7$ images). Twelve contiguous axial locations and approximately 40 breaths for Xe-CT studies are selected from the whole lung volumetric scan performed near end-expiration.

Images are acquired with the scanner set in ventilation triggering mode with 80 keV energy (for higher Xe signal enhancement), 160 mAs tube current, a 360° rotation, a 0.33 sec scan time, and 2.4 mm slice thickness. Respiratory gating is achieved by replacing the standard ECG gating signal with a trigger signal from a LabView program. Both of the two types of images are acquired with a matrix of 512 by 512 and without moving the animal between scans, so after acquisition the data sets are in rigid alignment.

### 2.2 Image Registration

Inverse consistent linear elastic image registration was applied to register phase change image pairs [10]. The registration estimates the inverse consistency error between the forward and reverse transformation, so it provides more accurate correspondences between two images compared to independent forward and reverse transformations. The registration minimizes the cost function defined as:

$$C = \sigma[C_{SIM}(I_0 \circ h, I_1) + C_{SIM}(I_1 \circ g, I_0)] + \tag{1}$$

$$\chi[C_{ICC}(u, \tilde{w}) + C_{ICC}(w, \tilde{u})] +$$

$$\rho[C_{REG}(u) + C_{REG}(w)],$$

where the forward transformation $h$ is used to deform the image $I_0$ into the shape of the image $I_1$, and the reverse transformation $g$ is used to deform the shape of $I_1$ into that of $I_0$. The deformed template and target images are denoted by $(I_0 \circ h)$ and $(I_1 \circ g)$, respectively. The vector displacement function $\boldsymbol{u}(x, y, z)$ that maps image $I_0$ to image $I_1$ is used to calculate the local lung expansion using the Jacobian determinant $J(x, y, z)$ defined as:

$$J(x,y,z) = \begin{vmatrix} 1 + \frac{\partial u_x(x,y,z)}{\partial x} & \frac{\partial u_x(x,y,z)}{\partial y} & \frac{\partial u_x(x,y,z)}{\partial z} \\ \frac{\partial u_y(x,y,z)}{\partial x} & 1 + \frac{\partial u_y(x,y,z)}{\partial y} & \frac{\partial u_y(x,y,z)}{\partial z} \\ \frac{\partial u_z(x,y,z)}{\partial x} & \frac{\partial u_z(x,y,z)}{\partial y} & 1 + \frac{\partial u_z(x,y,z)}{\partial z} \end{vmatrix},$$

where $u_x(x, y, z)$ is the $x$ component of $\boldsymbol{u}(x, y, z)$, $u_y(x, y, z)$ is the $y$ component of $\boldsymbol{u}(x, y, z)$, and $u_z(x, y, z)$ is the $z$ component of $\boldsymbol{u}(x, y, z)$.

The $C_{SIM}$ term of the cost function defines the symmetric intensity similarity. The $C_{ICC}$ term is the inverse consistency constraint or inverse consistency error cost and is minimized when the forward and reverse transformations are inverses of each other. The $C_{REG}$ term is used to regularize the forward and reverse displacement fields. The functions $u, w, \tilde{u}, \tilde{w}$ are voxel displacement fields and are related to the forward and reverse transformations by the equations: $h(x) = x + u(x)$, $g(x) = x + w(x)$, $h^{-1}(x) = x + \tilde{u}(x)$, $g^{-1}(x) = x + \tilde{w}(x)$. The constants $\sigma$, $\chi$ and $\rho$ are used to enforce/balance the constraints. In our registrations, we set the weighting constants $\sigma = 1$, $\chi = 600$, and $\rho = 0.00125$. The parameters were made on the basis of pilot experiments, previous work and experience.

The Jacobian measures the differential expansion at position $(x, y, z)$ in the image $I_1$. If the Jacobian is greater than one, there is local tissue expansion; if the Jacobian is less than one, there is local tissue contraction (Figure 1).

In our study, we register $T0$ to $T1$, $T1$ to $T2$, ..., and $T6$ to $T7$ in the dynamic respiratory-gated image sequence and thus acquire seven transformation pairs.

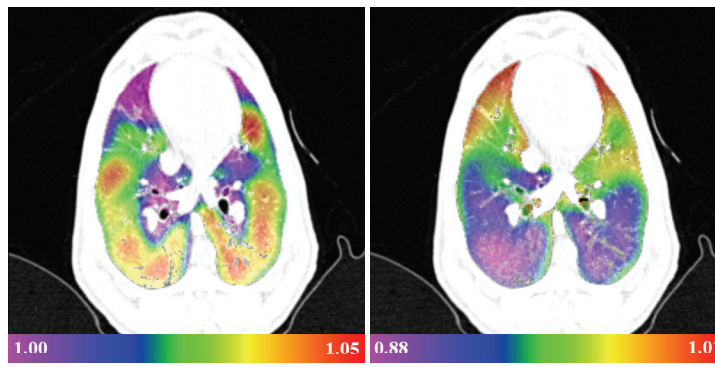


(a) (b)

**Fig. 1.** Color-coded maps showing (a) the Jacobian of the image registration transformation (unitless) for approximately the same anatomic slice computed from the $T0 - T1$ inspiration image pair and (b) the $T4 - T5$ expiration image pair. Note that the color scales are different for (a) and (b). Red regions on the inspiration image (a) are regions that have high expansion while dark blue regions on the expiration image (b) have high contraction.

### 2.3 Assessment of Image Registration Accuracy

For each dynamic respiratory-gated image sequence, 20 anatomic landmarks were matched across all eight image $T0$, ..., $T7$. The selected landmarks were recognizable branchpoints of the vascular and airway branches. For each landmark, the actual landmark position was compared to the registration-derived estimate of landmark position and the error was calculated.

### 2.4 Jacobian-Based Lung Expansion Compared to Lung Ventilation

Xe-CT estimates of specific ventilation (sV) are computed using the "time-series image analysis" (TSIA) software described in [9]. To compare the Jacobian values with the sV, we must identify corresponding regions in the two images. The Xe-CT has only twelve slices of axial coverage and the data sets are acquired in rigid

alignment as described in Section 2.1, so we register the twelve-slice Xe-CT data to the $T0$ whole-volume dynamic respiratory-gated CT data using rigid affine registration as shown in Figure 2. We subdivide the Xe-CT data into 30 slabs along the $y$ (ventral–dorsal) axis. We track the deformation of each slab across the sequence of volume images (i.e., from $T0$ to $T1$ to $T2$, etc.) and compare the average Jacobian within each slab to the corresponding average sV measurement in the Xe-CT images.

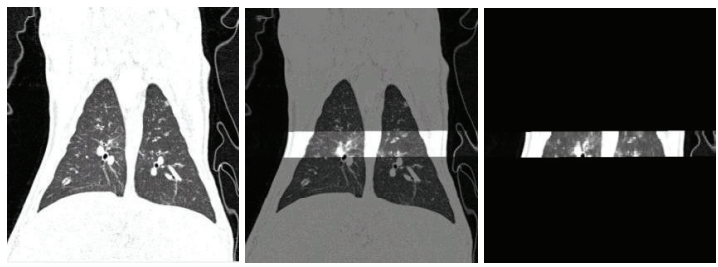

(a) (b) (c)

**Fig. 2.** Example of the result of affine registration between Xe-CT data and dynamic respiratory-gated CT data. (a) $T0$ whole-volume dynamic respiratory-gated CT data. (b) Fused image. (c) Deformed first breath of the Xe-CT data.

## 3 Results

### 3.1 Registration Accuracy

Figure 3a-b shows the projection of the manually-selected landmark locations onto coronal and sagittal slices for one animal. Figure 4 shows the registration accuracy as assessed by predicting the motion of the 20 manually-defined landmarks across seven phase change pairs. Overall the registration accuracy is on the order of 1 mm, or about 2 voxels.

### 3.2 Lung Expansion and Xe-CT Estimates of sV

Figure 5a shows the average Jacobian vs. lung height for all phase change pairs. Figure 5b shows the average sV vs. lung height calculated from the Xenon-CT study. Figure 6 shows average Jacobian vs. average sV at the $T0$ to $T1$ inspiration phase change pair and $T4$ to $T5$ expiration phase change pair. The figure gives the equation of the linear regression line with $r^2$ values and 95% confidence for the linear fits between average sV and the average Jacobian. Figure 7 shows the correlation coefficients $r^2$ from the linear regression of average Jacobian and sV

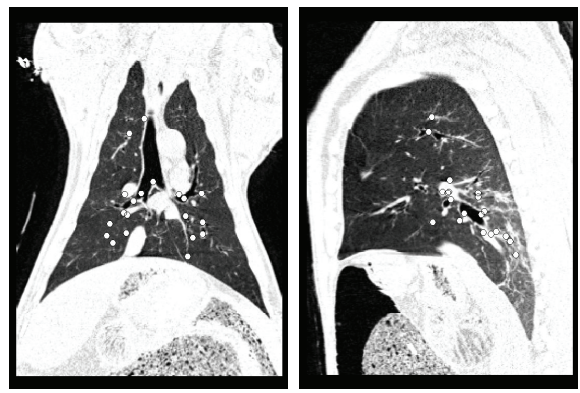

(a) (b)

**Fig. 3.** Manually-selected landmark locations projected onto (a) a coronal slice and (b) a sagittal slice for one animal at T0 breathing phase.

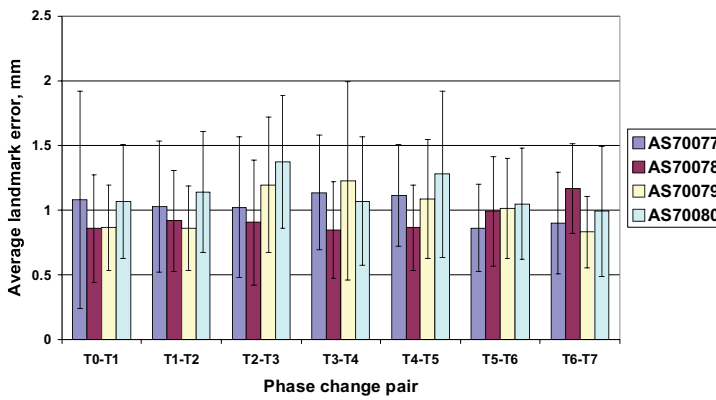


**Fig. 4.** Registration accuracy by mean ± standard deviation of landmark errors for each phase change pair and for each animal.

for each phase change pair and each animal. The phase change pair $T2$ to $T3$ shows the highest average correlation $r^2 = 0.85$ among all phase change pairs.

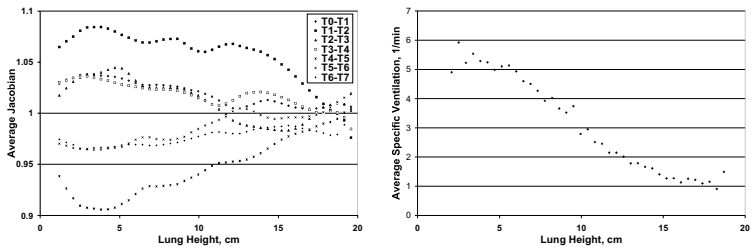


(a) (b)

**Fig. 5.** Example of Jacobian and sV measurements vs. lung height for one animal. (a) Average Jacobian values for all phase change pairs and (b) average sV vs. lung height. Lung height is 0 cm is the most dorsal position and positive heights move toward the ventral direction.

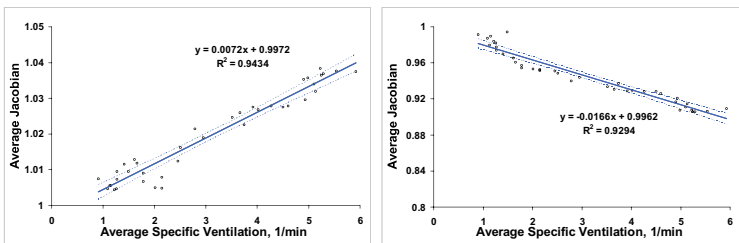


(a) (b)

**Fig. 6.** Examples of scatter plot of average sV and average Jacobian for one animal with linear regression with 95% confidence interval for (a) $T0$ to $T1$ phase change pair and (b) $T4$ to $T5$ phase change pair.

## 4 Discussion and Summary

We have calculated estimates of lung expansion from the Jacobian of the registration deformation field during tidal breathing for respiratory phase change

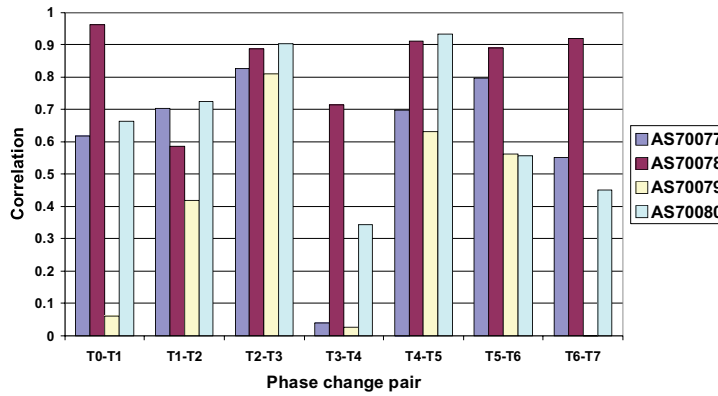


**Fig. 7.** Correlation coefficients $r^2$ from the linear regression of average Jacobian and sV for each phase change pair and for each animal.

pairs. The Jacobian values were compared to the Xe-CT based measures of specific ventilation. The correlation to the Xe-CT sV is higher for the Jacobian calculated from the dynamic respiratory-gated images ($r^2 = 0.84$) than for the static breath-hold images ($r^2 = 0.74$) as we reported [1]. The linear regression relationship in Figure 7 shows a wide range between animals and phases. We suspect it is caused by the natural anatomical difference between animals. Further more, since we used time based respiratory gating, the lung expand and contract differently between each phase change pair. For example, the lungs do not expand as much in $T3$ to $T4$ phase change pair as in $T2$ to $T3$ phase change pair. It would be interesting to determine if pressure based respiratory gating method will give better result.

The average registration error was about 1 mm in the phase change image pairs. Since the landmarks in these experiments were manually defined by picking anatomic features on a computer display, some component of this error is likely attributable to human error.

Since the Xe-CT data is collected over several breaths during tidal breathing, it is reasonable to expect that the Jacobian calculated from the dynamic respiratory-gated volume images would more closely reflect the ventilation patterns measured by the Xe-CT. The moving, breathing lung has mass, inertia, and hysteresis, and the true dynamics of the respiratory system are probably better revealed using images acquired across free breathing. Figure 8 shows the different arrival phases for different regions of the lung when largest expansion and largest contraction occur. Most of the lung regions will have the largest expansion at the middle phase ($T1$ to $T2$ or 25% to 50% of the inspiration du-

ration) and the largest contraction at the beginning phase ($T4$ to $T5$ or 100% to 75% of the expiration duration). It shows the lung does not expand or contract uniformly along the phases.

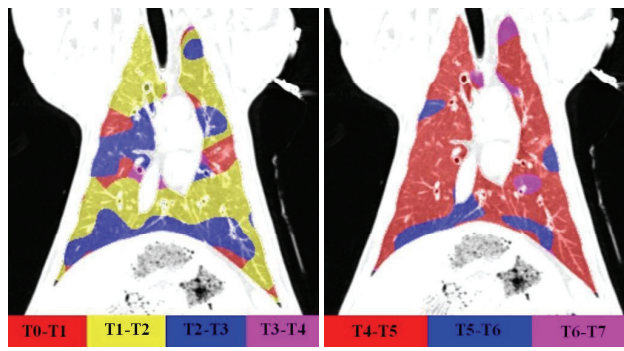


(a) (b)

**Fig. 8.** (a) Color coded image showing the (a) the phase point when largest expansion occur and (b) the largest contraction occur. Note the color scales are different for (a) and (b).

Additional work is needed to validate these methods before translation to use in humans. For imaging humans during normal respiration, the dynamic imaging may pose some challenges. The retrospectively reconstructed respiratory-gated images require regular and repeatable breathing patterns, so the subject must be trained to breath properly before images are acquired. In addition, since image data is gathered over several breaths and then reconstructed at different phases, the dynamic imaging will deliver more radiation dose than a single pair of breath-hold scans. The development of low dose imaging and/or *prospective* respiratory-gating may be able to reduce the radiation exposure. With the validation of the best correlated phase change pair during tidal breathing, the subject will only need to be scanned at two certain phases and the radiation dose will be significantly reduced.

If these methods can eventually be extended to humans, they would provide important new tools for studying the lung. Xe-CT requires the use of expensive xenon gas and the associated hardware to control delivery of the gas and harvest the gas from expired air for recycling. In addition, it is known that xenon gas has a strong anesthetic effect that must be carefully monitored. Finally, Xe-CT imaging protocols require high temporal resolution imaging, so typically axial coverage is limited to just a few slices at a time. However, if a registration-based analysis of images acquired during tidal breathing could be registered across

respiratory phase, high-resolution maps of lung expansion could be produced for the entire lung with low cost and dose.

## 5 Acknowledgments

This work was supported in part by grants HL079406, HL64368, HL080285, and EB004126 from the National Institutes of Health.

## References

1. Reinhardt, J.M., Ding, K., Cao, K., Christensen, G.E., Hoffman, E.A., Bodas, S.V.: Registration-based estimates of local lung tissue expansion compared to xenon-ct measures of specific ventilation. Medical Image Analysis (In press)
2. Guerrero, T., Sanders, K., Noyola-Martinez, J., Castillo, E., Zhang, Y., Tapia, R., Guerra, R., Borghero, Y., Komaki, R.: Quantification of regional ventilation from treatment planning CT. Int. J. Radiation Oncology Biol. Phys. **62**(3) (Jul 1 2005) 630–634
3. Guerrero, T., Sanders, K., Castillo, E., Zhang, Y., Bidaut, L., Komaki, T.P.R.: Dynamic ventilation imaging from four-dimensional computed tomography. Phys Med Biol. **51**(4) (Feb. 21 2006) 777–791
4. Gee, J., Sundaram, T., Hasegawa, I., Uematsu, H., Hatabu, H.: Characterization of regional pulmonary mechanics from serial magnetic resonance imaging data. Acad. Radiol. **10** (2003) 1147–1152
5. Christensen, G.E., Song, J.H., Lu, W., Naqa, I.E., Low, D.A.: Tracking lung tissue motion and expansion/compression with inverse consistent image registration and spirometry. Med Physics **34**(6) (June 2007) 2155–2165
6. Moller, H.E., Chen, X.J., Saam, B., Hagspiel, K.D., Johnson, G.A., Altes, T.A., de Lange, E.E., Kauczor, H.U.: MRI of the lungs using hyperpolarized noble gases. Magnetic Resonance in Medicine **47**(6) (2002) 1029–1051
7. Marcucci, C., Nyhan, D., Simon, B.A.: Distribution of pulmonary ventilation using Xe-enhanced computed tomography in prone and supine dogs. J. Applied Physiology **90**(2) (2001) 421–430
8. Tajik, J.K., Chon, D., Won, C.H., Tran, B.Q., Hoffman, E.A.: Subsecond multisection CT of regional pulmonary ventilation. Acad. Radiol. **9** (2002) 130–146
9. Chon, D., Simon, B.A., Beck, K.C., Shikata, H., Saba, O.I., Won, C., Hoffman, E.A.: Differences in regional wash-in and wash-out time constants for xenon-CT ventilation studies. Respiratory Physiology & Neurobiology **148** (2005) 65–83
10. Christensen, G., Johnson, H.: Consistent image registration. IEEE Transactions on Medical Imaging **20**(7) (July 2001) 568–582